Effects of Molecular Orientation on the Electronic Structure of fcc C60

doi: 10.1103/PhysRevB.49.16202

Effects of molecular orientation on the electronic structure of fcc C_{60}

Bing-Lin Gu
Institute for Materials Research, Tohoku University, Sendai, 980, Japan
and Department of Physics, Tsinghua University, Beijing, China

Yutaka Maruyama, Jing-Zhi Yu, Kaoru Ohno, and Yoshiyuki Kawazoe
Institute for Materials Research, Tohoku University, Sendai, 980, Japan
(Received 5 November 1993; revised manuscript received 2 February 1994)

We have investigated the effects of C_{60} molecular orientation on the electronic structure of fcc C_{60} solids by performing a band-structure calculation with self-consistent mixed-basis all-electron and full-potential approach within the local-density approximation. The degeneracies at special k points, the dispersion, and the widths of bands and the location of the valence-band maximum and the conduction-band minimum have been found to be sensitive to the orientation of the fullerenes in fcc lattices.

I. INTRODUCTION

The electronic structure of the fullerites has been the subject of numerous experimental and theoretical investigations since the discovery and practical synthesis of this form of carbon.[1,2] Nevertheless, some fundamental issues remain unsolved, even in the case of pure solid C_{60}.

As we know, a rapid rotation of C_{60} (10^9/sec) in this crystal has already been found to occur even at room temperature[3] and the C_{60} molecules are orientationally disordered and the crystal structure may be regarded as a face-centered-cubic configuration. Below 260 K, however, the molecules become orientationally ordered and a simple-cubic lattice results.[4–7] Moreover, the successful growth of oriented C_{60} fullerite layers on substrates has been reported.[8–11] Themlin *et al.*[8] have found the natural one-dimensional corrugation of the (001) cleavage plane of GeS allows the growth of C_{60} (111) fullerite layers. Hashizume *et al.*[9,10] have observed firstly the different patterns of electronic partial charge densities of C_{60} layers deposited on Si(100) and Cu(111) surfaces. The band-structure variation depending upon the orientation of C_{60} will become a very important subject in physics and materials science of solid fullerenes.

Saito and Oshiyama[12] have calculated the band structure of an fcc C_{60} crystal using the norm-conserving nonlocal pseudopotentials and a Gaussian-orbital basis set, and concluded that it is a semiconductor with a direct energy gap of 1.5 eV at the X point, and the width of the top valence band is 0.42 eV. In their calculation, each crystal axis crosses the double bond at the midpoint.

Troullier and Martins[13] have also calculated the band structure of an fcc C_{60} using "soft" pseudopotential local-density calculations with plane waves; their results are quite different from the results of a local-density calculation with a Gaussian basis set by Saito and Oshiyama;[12] the width of the top valence band is 0.58 instead 0.42 eV, and the gap is 1.18 instead 1.5 eV.

Recently, Shirley and Louie[14] have found the band gap of 2.15 eV and about 1 eV widths for the highest-occupied-molecular-orbital (HOMO) and lowest-unoccupied-molecular-orbital (LUMO) bands using a quasiparticle approach, and suggested that the solid C_{60} is a standard band insulator.

This paper focuses on the effects of molecular orientation on electronic structure and charge distributions. Here we would like to treat the fullerene molecules as accurately as possible, because the effects depend on the fine structures in the crystal and should be considered in detail. Therefore, we have chosen a self-consistent mixed-basis all-electron and full-potential approach within the local-density approximation (LDA). The band-structure calculation is carried out in the following three cases. First, we adopted the same orientation of the fullerene as those of Saito and Oshiyama[12] and Troullier and Martins,[13] i.e., the molecular unit is oriented in the highest possible symmetry T_h^3, as shown in Fig. 1(a). In this choice of the orientation of the C_{60} molecule of fcc lattice sites, each molecule has 12 equivalent nearest-neighbor molecules, then, each pentagon in a C_{60} molecule has two C atoms, which are nearest to the neighboring C_{60} molecule. In this case, the results agreed remarkably well with those of Troullier and Martins.[13] Second, we have rotated the C_{60} molecule by 90° with respect to the $\langle 001 \rangle$ crystallographic axis [see Fig. 1(b)] and then calculated the electronic structure. As expected, similar results as in case 1 have been obtained. Third, we have placed the C_{60} molecule so that one of the ten threefold icosahedral axes is aligned with one of the crystallographic axis [see Fig. 1(c)]. We have found that this change in the orientation causes considerable change on the band structure of fcc C_{60}. The conduction-band minimum occurs at the L point in k space and the valence-band maximum at the W point. Accordingly, the energy gap is an indirect one. The degeneracies at the special k points are also remarkably changed.

This paper is organized as follows. In Sec. II, the method of the present calculation is briefly described. In

Sec. III, the numerical results of band structure and charge distribution of fcc C_{60} are presented in the above three different cases, and the influence of the rotation of the fullerenes on the electronic structures is reported. The conclusion is given in Sec. IV.

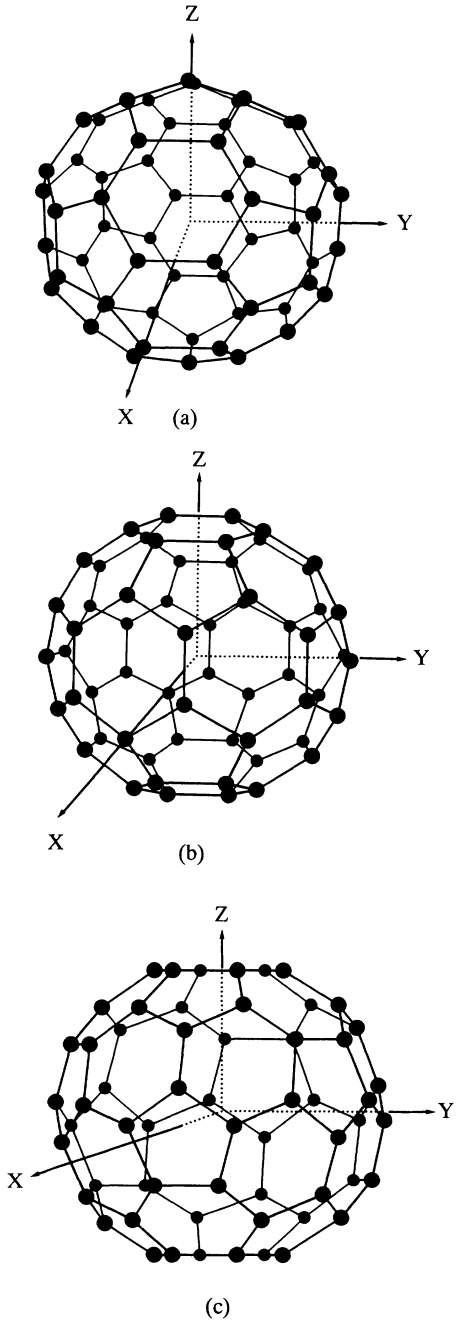

FIG. 1. Atomic positions in the solid fcc C_{60}. (a) Each crystal axis crosses the double bond at the midpoint; this choice maintains the highest possible symmetry between the icosahedral symmetry of the C_{60} molecular units and the fcc lattice (case 1); (b) in contrast to case 1, the C_{60} molecule is rotated 90° with respect to the ⟨001⟩ crystallographic axis (case 2); (c) one of the ten threefold icosahedral axes of the C_{60} molecule is aligned with one of the crystallographic axis (case 3).

II. SELF-CONSISTENT MIXED-BASIS FULL-POTENTIAL APPROACH

The mixed-basis method was introduced by Louie, Ho, and Cohen[15] for the calculation of the electronic structure of solids. A combined set of plane waves and Bloch

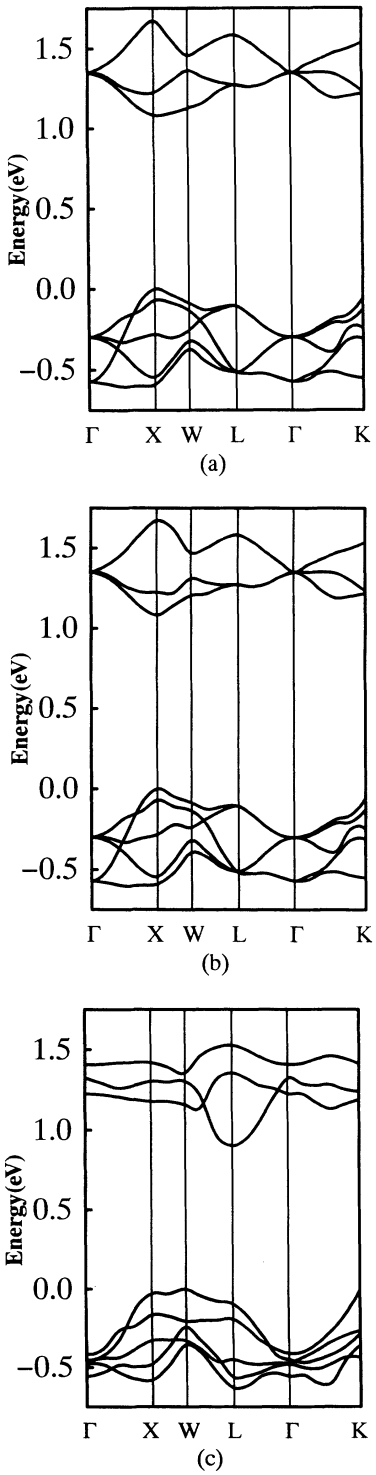

FIG. 2. The calculated HOMO and LUMO band structures for (a) case 1, (b) case 2, and (c) case 3.

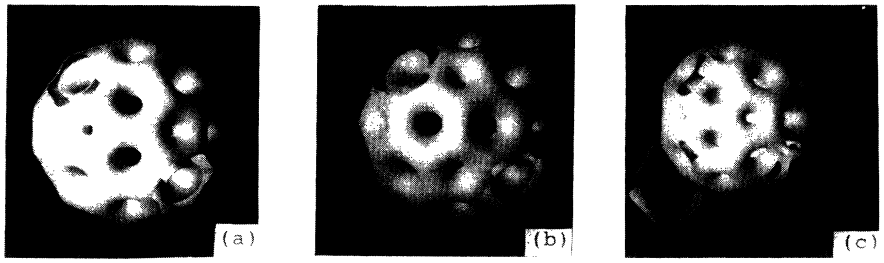

FIG. 3. The spatial distributions of total charge density of fcc C_{60} inside the unit cell. (a) corresponds to case 1, (b) to case 2, and (c) to case 3, respectively.

sums of localized functions is employed as basis functions, thus leading to a very efficient representation of the system, which contains both highly localized (atomiclike) and delocalized (plane-wave-like) electrons.

The present method is based on the density-functional theory and LDA with a full potential. This method has been discussed in detail elsewhere.[16] The main point of this method is as follows.

The basis set $|l\rangle$ consists of plane waves

$$\frac{1}{\sqrt{\Omega}} e^{i(\mathbf{k}+\mathbf{K})\cdot\mathbf{r}} , \tag{1}$$

and Bloch sums of local orbitals

$$\Phi_{i\mu}(\mathbf{k},\mathbf{r}) = \frac{1}{\sqrt{\Omega}} \sum_{R_m} e^{i\mathbf{k}\cdot(\mathbf{R}_m+\tau_i)} f_{i\mu}(r-\mathbf{R}_m-\tau_i) , \tag{2}$$

where $\mathbf{K}$ is a reciprocal-lattice vector, $\mathbf{R}$ a primitive vector, τ_i a basis vector, μ a label for the orbitals on the ith atom, Ω the crystal volume, and the localized functions $f_{i\mu}(\mathbf{r})$ are chosen as $1s$, $2p_x$, $2p_y$, and $2p_z$.

The electron wave function is expressed by

$$\Psi_{\mathbf{k}}(\mathbf{r}) = \frac{1}{\sqrt{\Omega}} \sum_{\mathbf{K}} A(\mathbf{k}+\mathbf{K}) e^{i(\mathbf{k}+\mathbf{K})\cdot\mathbf{r}} + \sum_{i\mu} \beta_{i\mu}(\mathbf{k}) \Phi_{i\mu}(\mathbf{k},\mathbf{r}) . \tag{3}$$

Since the atomic wave functions are not orthogonal with plane waves, a modified equation that guarantees the orthogonality becomes

$$H\Psi_i = (\Psi_i^{\dagger} H \Psi_i) S \Psi_i , \tag{4}$$

where

$$S = \langle k | l \rangle \tag{5}$$

is the overlap matrix of the wave functions. Introducing the lower half triangular matrix U, which satisfies

$$S = UU^{\dagger} , \tag{6}$$

and introducing

$$U^{\dagger}\Psi_i = \phi_i \quad \text{and} \quad H' = U^{-1} H U^{\dagger -1} , \tag{7}$$

we have

$$H'\phi_i = (\phi_i H' \phi_i)\phi_i . \tag{8}$$

To evaluate the charge density, one needs to trace the wave functions to those in the original nondiagonal form,

$$\Psi_i = U^{\dagger -1}\phi_i , \tag{9}$$

and

$$\rho(r) = \sum_{i}^{\text{occ}} |\Psi_i|^2 . \tag{10}$$

In the calculation of electronic structure, we take the two kinds of C-C bond lengths in the C_{60} cage, i.e., 1.46 Å on pentagons and 1.40 Å on neighboring hexagons. The lattice constant is chosen to be $a = 14.2$ Å, so that the nearest-neighbor distance of the C_{60} molecule in fcc C_{60} is fit to the experimental value of 10.0 Å.[4]

As a basis set of the electron wave function, 60 $1s$ and 60 $2p_x$, 60 $2p_y$, 60 $2p_z$ atomic orbitals of C_{60}, and 2109 plane waves are adopted. The exponential damping factors α and β for the $1s$ and $2p$ atomic wave functions are chosen as $\alpha = 1/0.106$, and $\beta = 1/0.133$ Å^{-1}, respectively. The real space is divided into $64\times64\times64$ meshes where 3.185 meshes correspond approximately to 1 a.u. = 0.529 Å.

For the computation, we used the NEC SX-3 supercomputer in the Osaka University Computing Center. The energies and wave functions of the electrons are obtained by the standard self-consistent iteration computation, which uses matrix diagonalization and mixes the

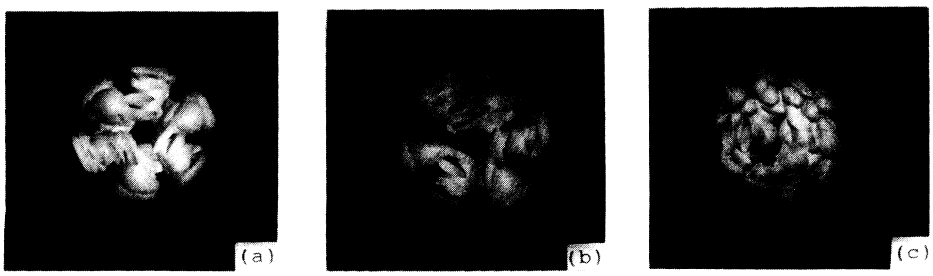

FIG. 4. The charge density for the 180th level. (a) corresponds to case 1, (b) to case 2, and (c) to case 3, respectively.

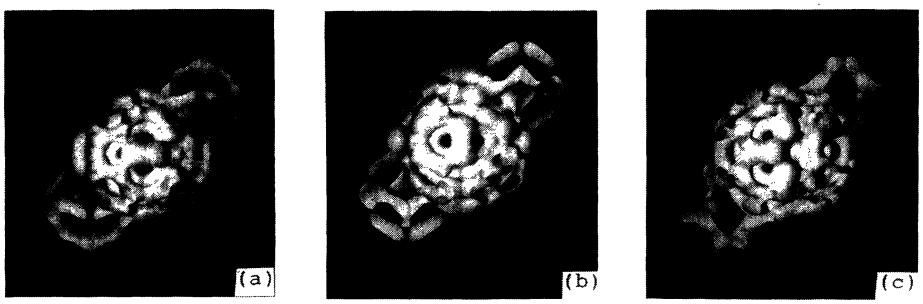

FIG. 5. The spatial distributions of the sum of the highest-occupied valence orbitals (176–180). (a) corresponds to case 1, (b) to case 2, and (c) to case 3, respectively.

charge density of the previous step; 26 iterations were performed for the convergence.

III. RESULTS AND DISCUSSION

We have calculated the band structure of fcc C_{60} in three different orientational cases. Figure 2(a) shows the calculated HOMO and LUMO band structures for fcc-T_h^3 geometry corresponding to case 1(a). Since we know that the highest-occupied state of the C_{60} molecule is the h_u symmetry, this level is split by the tetrahedral crystal field into a t_u and an e_u state at the Γ point and forms five dispersive bands. Both the valence-band maximum and conduction-band minimum are located at the X point. The band gap is 1.10 eV. The widths for HOMO (H_u), LUMO (T_{1u}), and next higher (T_{1g}) complexes of bands near the gap are 0.59, 0.59, and 0.56 eV, respectively, exhibiting a 30% enhancement of bandwidths as compared to the results by Saito and Oshiyama.[12] The present mixed-basis LDA results agree remarkably well with those of Troullier and Martins.[13] Figure 2(b) shows the calculated band structure corresponding to case 2, in which we placed the molecules in an fcc lattice and set them in the orientation to obtain also a tetrahedral space group T_h^3. As expected, similar results as in case 1 have been obtained. However, the details of the band dispersion from X-W-L are somewhat different.

Figure 2(c) shows the calculated HOMO and LUMO band structures corresponding to case 3. The present calculation with this case gives a typical example of the influence of the orientation on the band structures in fcc C_{60}. We have found that the rotation causes considerable change on the band structure of fcc C_{60}. At the Γ point, the highest-occupied state of the C_{60} molecule is split into two single states and a triplet (T_u) state, and both LUMO (T_{1u}) and next higher (T_{1g}) complexes of bands are split into three single states, respectively. The computed widths for the HOMO (H_u), LUMO (T_{1u}), and next higher (T_{1g}) complexes of bands near the gap are 0.6, 0.6, and 0.58 eV, respectively, and the dispersions of the bands are broader than more symmetrical ones. Surprisingly, the valence-band top moves to the W point, and the conduction-band bottom moves to the L point. The fcc C_{60} crystal becomes an indirect-gap semiconductor with an energy gap of 0.9 eV.

Figures 3(a), 3(b), and 3(c) indicate the spatial distributions of total charge densities of fcc C_{60} inside the unit cell corresponding to cases 1, 2, and 3, respectively. These figures show isosurfaces with the same electron density, which was taken appropriately. There are net charge densities around the intermolecular region in all cases. In case 3, there is even notable extra charge density in the interstitial region. One can make a qualitative observation that the electronic distribution in case 3 is not so much concentrated in the vicinity of the C-ion cores compared to case 1 and 2. This feature does not change even if we look at isosurfaces with a somewhat different value of electron charge density. As far as we know, an appreciable overlap of atomic waves functions suggests the presence of broader bands. This is why the dispersions of bands corresponding to case 3 are broader than those corresponding to cases 1 and 2.

To understand the split of the energy level at the Γ point, the charge density for 180th level is shown in Fig. 4 on the $\langle 111 \rangle$ direction. Three kinds of oriented molecules form the fcc lattice, respectively, and all of them have the same translational symmetry through Bravais lattice vectors, but they do not have the same point-group symmetry due to different orientations in the lattice. In cases 1 and 2, the wave functions maintain the highest possible symmetry T_h^3, while in case 3, the wave-function symmetry becomes lower and it loses the degeneracies at the special k points.

We next show the spatial distribution of the partial

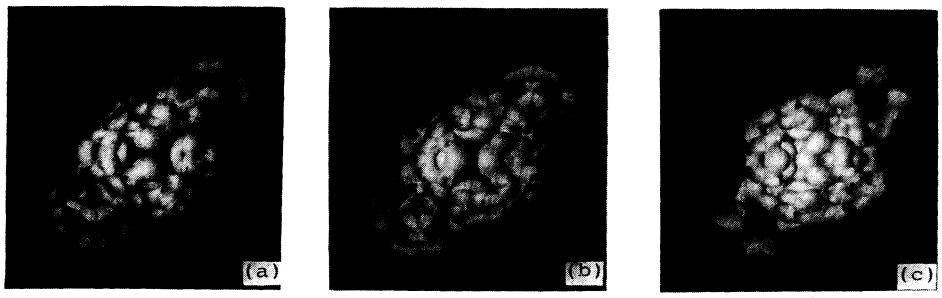

FIG. 6. The spatial distributions of the sum of the lowest-unoccupied conduction orbitals (181–183). (a) corresponds to case 1, (b) to case 2, and (c) to case 3, respectively.

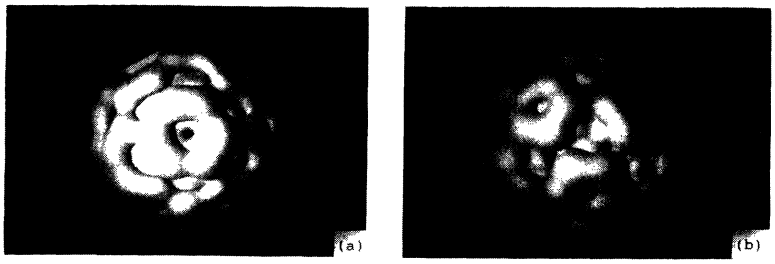

FIG. 7. Top view of the spatial distribution of partial charge density (a) valence electrons (176–180) and (b) conduction electrons (181–183), corresponding to case 3.

charge density of HOMO (H_u) and LUMO (T_{1u}). Figure 5 is for the highest-occupied valence orbitals (176–180). It is clearly shown that most charge is located at the double bonds. There is a nonlocalized electronic cloud around the interstitial region. In contrast to valence electron distribution, the electrons in the lowest-unoccupied molecular orbitals [shown in Fig. 6 for 181–183 (T_{1u})] are located more at single bonds than double bonds, and spread more and more as an extended electronic cloud to the interstitial region.

Troullier and Martins[13] have also given the charge density in contour plots of the wave function instead of the three-dimensional presentation in this paper. Comparing the two results, their basis features are nearly the same as ours, especially for the $60° \leq \theta \leq 120°$ region.[4]

It is very important to compare our theoretical calculation with the experimental results. Recently, the charge distribution can be accurately measured by scanning tunneling microscopy (STM). Hashizume *et al.*[9,10] have observed that bias voltage-dependent STM images of individual C_{60} molecules show unique intramolecular structures. When the bias voltage is $V_b = -2.0$ eV, the C_{60} molecular image appears in a doughnut shape, almost round with a hole at the center; when the bias voltage $V_b = 2.0$ V, an image with threefold symmetry appears evidently.

According to our calculation, the STM image at $V_b = -2.0$ V should correspond to the charge density of the valence electron, the six ring with three short bonds in doughnut shape should be observed [as shown in Fig. 7(a)]. On the contrary, the charge density of the conduction electron should be observed at $V_b = 2.0$ V [as shown in Fig. 7(b)]. It is quite understandable when $V_b = -2.0$ V, the valence electron flows from C_{60} to the STM tip; on the other hand, when $V_b = 2.0$ V, the electron flows from the tip to the conduction band of C_{60}. The calculated charge densities agree well with those observed images by STM (Ref. 13) (see Fig. 2 of Ref. 13).

IV. CONCLUSION

We have investigated the effects of molecular orientation on the electronic structure of fcc C_{60} by performing a self-consistent mixed-basis all-electron and full-potential band-structure calculation within the local-density approximation for three different orientations of C_{60} in the fcc crystal. We have found that the orientation causes considerable change on the electronic structure of fcc C_{60}.

ACKNOWLEDGMENTS

One of the authors (B.L.G.) gratefully acknowledges the support by Hitachi. This work has partially been supported by an IBM Partnership Program and the Grant-in-Aid of the Ministry of Education, Science and Culture of Japan.

[1]H. W. Kroto, J. R. Heath, S. C. O'Brien, R. E. Curl, and R. E. Smalley, Nature (London) **318**, 162 (1985).
[2]W. Krätschmer, L. D. Lamb, K. Fostiropocclos, and D. R. Hoffman, Nature (London) **347**, 354 (1990).
[3]C. S. Yannoni, J. Phys. Chem. **95**, 9 (1991).
[4]P. A. Heiney, J. E. Fishcher, A. R. McGhie, W. J. Romanow, A. M. Denenstein, J. P. McCauley, Jr., A. B. Smith III, and D. E. Cox, Phys. Rev. Lett. **66**, 2911 (1991).
[5]R. Tycko, G. Dabbagh, R. M. Fleming, R. C. Haddon, A. V. Makkija, and S. M. Zahurak, Phys. Rev. Lett. **67**, 1886 (1991).
[6]W. I. F. David, R. M. Ibberson, J. C. Matthewman, K. Prassides, T. J. S. Dennis, J. P. Have, H. W. Kroto, R. Taylor, and D. R. M. Walton, Nature (London) **353**, 147 (1991).
[7]R. D. Johnson, C. S. Yannoni, H. C. Dorn, J. R. Salem, and D. S. Bethune, Science **255**, 1235 (1992).
[8]J.-M Themlin, S. Bouzidi, F. Coletti, J.-M. Debever, G. Gensterblum, Li-Ming Yu, J.-J. Pireaux, and P. A. Thiry, Phys. Rev. B **46**, 15 602 (1992).
[9]T. Hashizume, X.-D. Wang, Y. Nishina, H. Shinohara, Y. Saito, Y. Kuk, and T. Sakurai, Jpn. J. Appl. Phys. **31**, L880 (1992).
[10]T. Hashizume, K. Motai, W. D. Wang, N. Shinohara, Y. Saito, Y. Maruyama, K. Ohno, Y. Kawazoe, Y. Nishina, H. W. Pickering, Y. Kuk, and T. Sakurai, Phys. Rev. Lett. **71**, 2959 (1993).
[11]L. D. Lamb, D. R. Hoffman, R. K. Workman, S. Howells, T. Chen, D. Sarid, and R. F. Ziolo, Science **255**, 1413 (1992).
[12]S. Saito and A. Oshiyama, Phys. Rev. Lett. **66**, 2637 (1991).
[13]N. Troullier and José Luis Martins, Phys. Rev. B **46**, 1754 (1992).
[14]E. L. Shirley and S. G. Louie, Phys. Rev. Lett. **71**, 133 (1993).
[15]S. G. Louie, K. M. Ho, and M. L. Cohen, Phys. Rev. B **19**, 1774 (1979).
[16]Y. Kawazoe, H. Kamiyama, Y. Maruyama, and K. Ohno, Jpn. J. Apl. Phys. **32**, 1433 (1993).

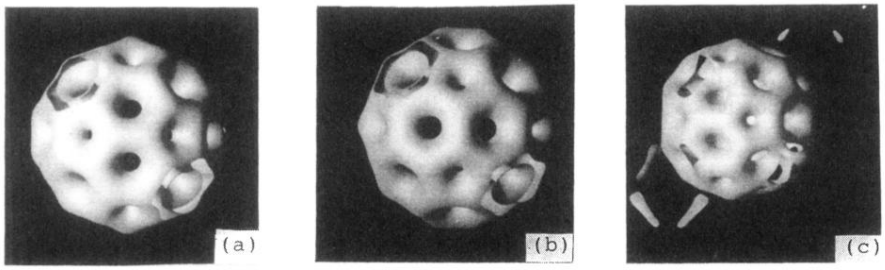

FIG. 3. The spatial distributions of total charge density of fcc C_{60} inside the unit cell. (a) corresponds to case 1, (b) to case 2, and (c) to case 3, respectively.

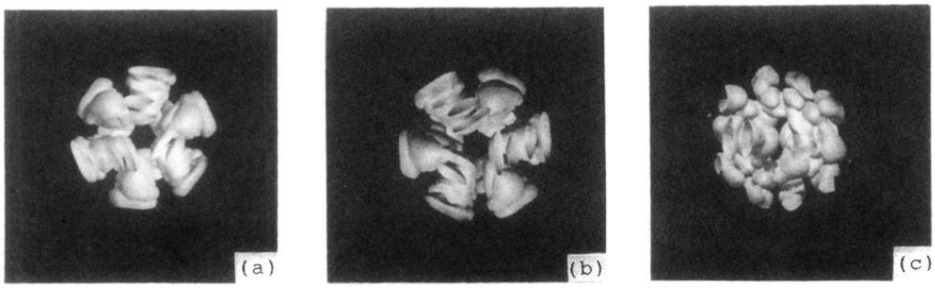

FIG. 4. The charge density for the 180th level. (a) corresponds to case 1, (b) to case 2, and (c) to case 3, respectively.

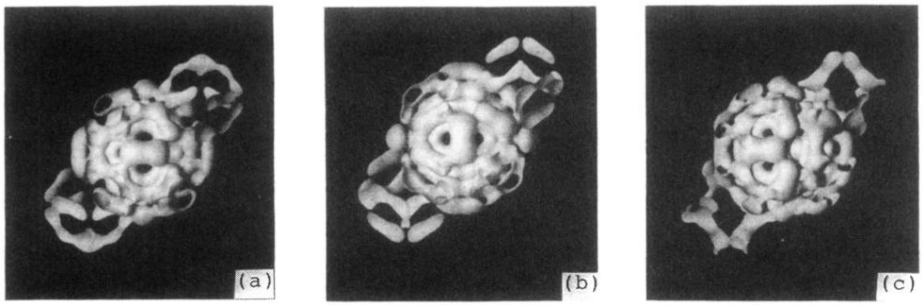

FIG. 5. The spatial distributions of the sum of the highest-occupied valence orbitals (176–180). (a) corresponds to case 1, (b) to case 2, and (c) to case 3, respectively.

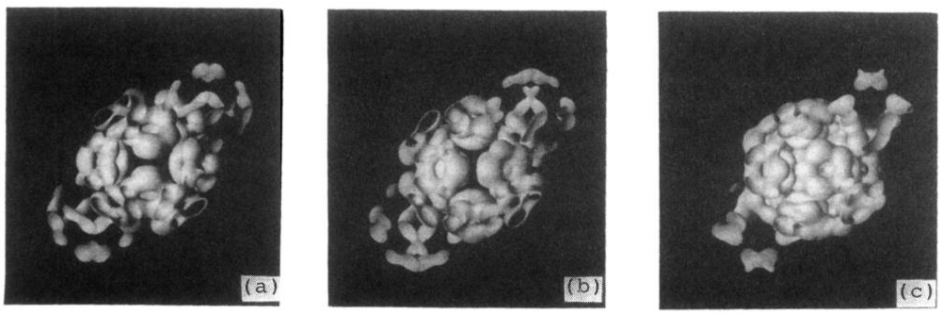

FIG. 6. The spatial distributions of the sum of the lowest-unoccupied conduction orbitals (181–183). (a) corresponds to case 1, (b) to case 2, and (c) to case 3, respectively.

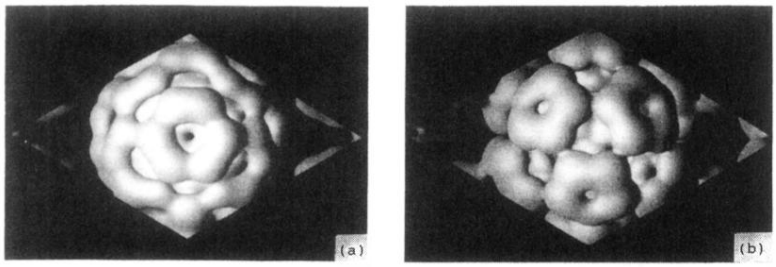

FIG. 7. Top view of the spatial distribution of partial charge density (a) valence electrons (176–180) and (b) conduction electrons (181–183), corresponding to case 3.